PERFORMANCE OF HEAT RESISTANT 13CrMo4 4 STEEL UNDER HIGH TEMPERATURE OXIDATION

F.J. Pérez, M.P. Hierro, C. Gómez* and F. Pedraza

Universidad Complutense de Madrid. Facultad de CC. Químicas. Dpto. de CC. Materiales e Ing. Metalúrgica. Madrid 28040. Spain

ABSTRACT

Heat resistant steel 13CrMo4 4 steel is extensively employed in fossil fuel-fired boilers. Its temperature of operation is rarely higher than about 525°C. In this study, the high temperature behaviour of this steel is being investigated under isothermal conditions, ranging from 400 to 800° C for a maximum exposure time of 300 hours in air. The oxidation results show that this alloy is able to withstand temperatures up to 600° C thanks to the formation of an oxide scale mainly based on haematite oxides, giving rise to a parabolic kinetics as a result of a solid state diffusion process. However, oxidation at 800° C brings about spalling of the oxide scale, changing from a parabolic to a paralinear law.

INTRODUCTION

Heat-resistant steels are widely employed in the manufacture of different equipments and installations designed for high temperature operations in the chemical, petrochemical, metallurgical and ceramics industries, as well as in the technology of waste gas processing. Applications include, for example, radiation tubes, supporting beams in furnaces, protective tubes for temperature-measuring devices as well as automobile exhaust gas cleaning systems /1,2/.

Specifically, 13CrMo 44 steel is used in a variety of applications that involve exposure to elevated temperatures and, possibly, reactive

*corresponding author: cgcastro@eucmos.sim.ucm.es

environments, such as collectors, water boilers and superheater tubes at temperatures below 530°C /3/. For the particular case of fossil-fired boilers, the steam temperature and, therefore, the metal temperature increases from the saturated steam temperature entering the superheater to the finishing temperature, consequently changing the permitted materials of construction.

The finishing sections of the tubing and the pipes that take the steam to the high pressure turbine are typically manufactured from low-alloy ferritic steels, such as 13CrMo4 4, in most cases, or austenitic steels, such as AISI 304, when the materials operate under higher mechanical loads during service /4/. These first-generation monotube boilers were operated in the subcritical regime with steam conditions below 186 bar and 540° C. The mechanical properties of these ferritic steels were sufficiently well-known and approved so that a safety factor of 100,000 h creep rupture strength was the main constraint. By now, all the properties of such ferritic materials are well established and a design for a lifetime of 200,000 h is the average /5/. However, nowadays, a number of advanced steels for steam power plant applications have been developed /6,7/ in an attempt to improve the corrosion and mechanical resistance. In such conditions, an understanding of their oxidation behaviour is essential for an effective life prediction design and possible future applications. In this sense, the study of a traditional heat-resistant steel may be interesting for purposes of comparison.

In the present work, the conventional 13CrMo4 4 steel has been subjected to a study of its corrosion kinetics at high temperatures, ranging from 400 to 800° C, for 300 hours of exposure. The kinetic laws governing the oxidation processes at each temperature are thus presented and subsequently explained on the basis of the microstructural changes, morphologies and compositions of the oxide layers formed on the surface.

EXPERIMENTAL

The as-received 13CrMo4 4 steel was in the form of a 3.4 (external) and 2.9 (internal) mm diameter pipeline, normally employed in the power plant of La Robla (Spain). The nominal compositions are given in Table 1. In order to evaluate the oxidation process on the as-received steel, a preliminary microstructural characterisation was carried out. For this purpose, the pipeline was machined to achieve square samples of about 1 cm^2, which were subsequently ground and polished with diamond paste up to 3 μm. The

Table 1
Chemical composition range of 13CrMo4 4 heat-resistant steel

	C	Si	Mn	P	S	Cr	Mo	Cu
Min (wt%)	0.08	0.10	0.40	-	-	0.70	0.40	-
Max. (wt%)	0.18	0.35	1.00	0.035	0.030	1.10	0.60	0.30

samples were then chemically etched with 2% Nital. The phases present in the steel were analysed by X-ray diffraction.

For the oxidation tests, rectangular (2x0.5x12 mm) specimens were obtained from the pipeline and ground up to a SiC#600 emery paper, washed and subsequently cleaned in acetone. The experimental equipment was a Setaram Gravitronic thermobalance, in which a continuous change in weight is registered as a function of time to obtain the kinetics law. The oxidation tests were carried out under atmospheric air pressure up to 300 h at 400, 600 and 800° C. Characterisation of the oxidised products was carried out by X-ray diffraction (XRD), scanning electron microscopy (SEM) coupled with EDS microanalyses and electron probe microanalysis (EPMA).

RESULTS AND DISCUSSION

SEM examination of the as-received steel showed a homogeneous ferritic-perlitic microstructure, as shown in Figure 1a. No differences in the shape and size of the grains along and across the pipeline axis were observed. The XRD patterns revealed that ferrite and cementite are the main phases of the as-received steel (Figure 1b).

Figure 2 shows the mass gain versus time after oxidation in air for up to 300 hours at 400, 600 and 800° C. It can be readily observed that this steel approaches a parabolic law both at 400 and at 600° C. However, at the highest temperature tested, the kinetics behaviour shows a quasi paralinear corrosion law, with an exponent higher than 0.5 $mg \cdot cm^{-2} \cdot h^{-1}$ already at the beginning. After this first period, the oxidation behaviour turns into a linear law, which gives rise to a dramatic increase in the oxygen intake and overall, the average mass gain is 0. 347 $mg \cdot cm^{-2} \cdot h^{-1}$ after 300 hours of exposure.

The X-ray diffractograms of Figure 3 show that the main phases are Fe_2O_3, Fe_3O_4 and small amounts of a body-centered cubic lattice

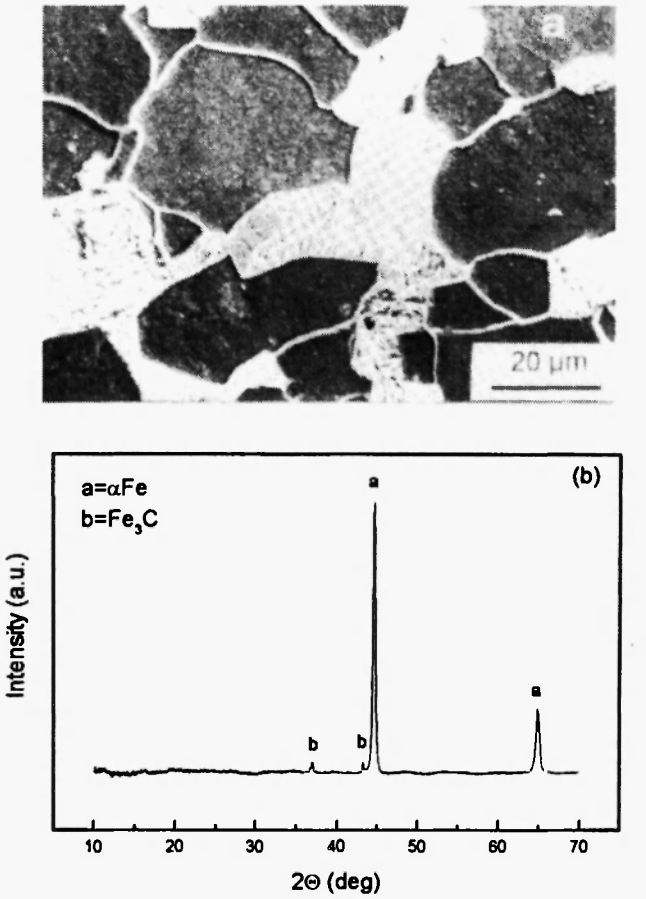

Fig. 1: Characterisation of the as-received steel a) microstructure and b) X-Ray diffractogram.

corresponding to that of the matrix in the specimens oxidised at the lowest temperatures. These results suggest a low thickness of the oxide scale grown under such conditions. Moreover, in the specimens oxidised at 800° C the main phase detected was $Fe_{1.2}Cr_{0.8}O_3$. Incorporation of Cr in the oxide scale could be due to a higher mobility of this cation at this temperature. However, $Fe(Fe,Cr)_2O_4$ spinel oxides have been earlier referenced under isothermal conditions /8/. Those authors suggested that in steels with chromium contents lower than about 20%, mixed spinels of iron and chromium could be formed

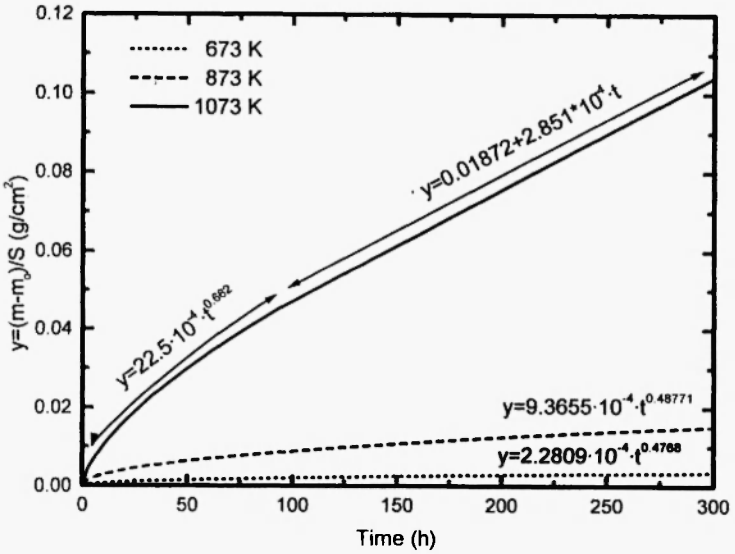

Fig. 2: Mass gain of 13CrMo4 4 versus time at the three tested temperatures.

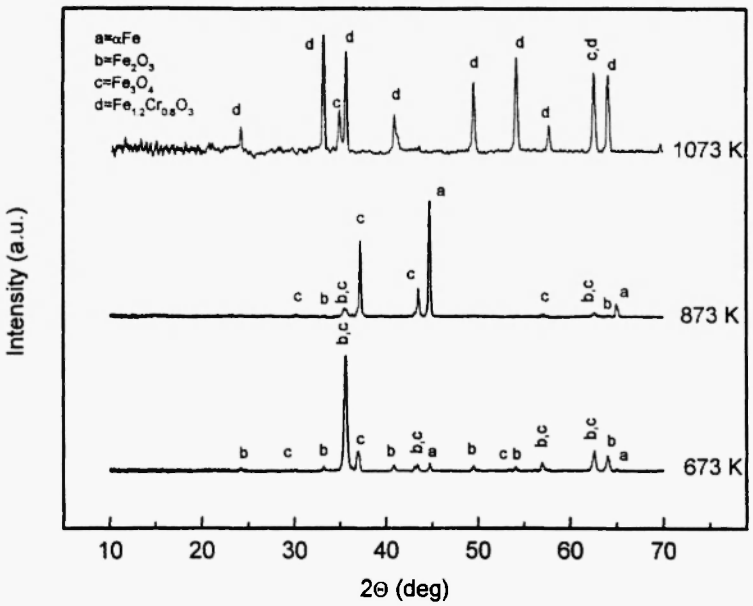

Fig. 3: Diffractograms of the oxidised samples at 400, 600 and 800° C.

at the metal-oxide interface, whereas the haematite Fe_2O_3 oxide could be formed at the oxide/air interface due to the fast diffusion of iron through this mixed spinel.

It is very likely that at the highest temperature of oxidation, i.e. 800° C, formation of wustite, FeO, had taken place. However, it must have been transformed into Fe-α and Fe_3O_4 upon cooling and thus wustite has not been detected in the X-ray analyses /9/. The same argument may apply to the specimens oxidised at 600° C, even though this is a limiting temperature for the formation of FeO because of the presence of small amounts of Cr. It is well known that incorporation of a cation with a smaller ionic radius than that of Fe^{2+} raises the high temperature limit of formation of wustite, FeO /10/. However, this did not happen in our case since α-Fe together with Fe_3O_4 was identified (see Fig. 3).

A thin and uniform oxide scale was grown on the sample treated at 400°C. Inspection of this scale at high magnifications showed small zones with some spallation, as shown in Figure 4, in which needle-like crystals growth are observed. On the contrary, specimens oxidised at 600° C exhibit a granular non-continuous oxide scale (Figure 5). Large oxide crystals covering the original alloy and the grain boundaries can be observed. The grain boundaries of this layer have an open morphology that could act as short-circuit paths for inward diffusion of oxygen /11/. When the oxidation temperature is increased

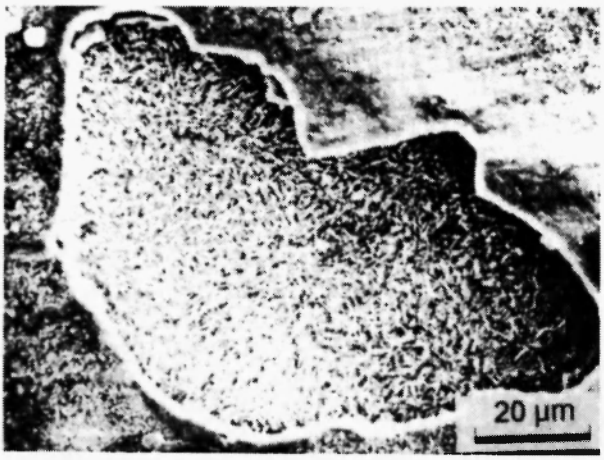

Fig. 4: SEM surface morphology of the sample treated at 400° C. Detail of some spallation.

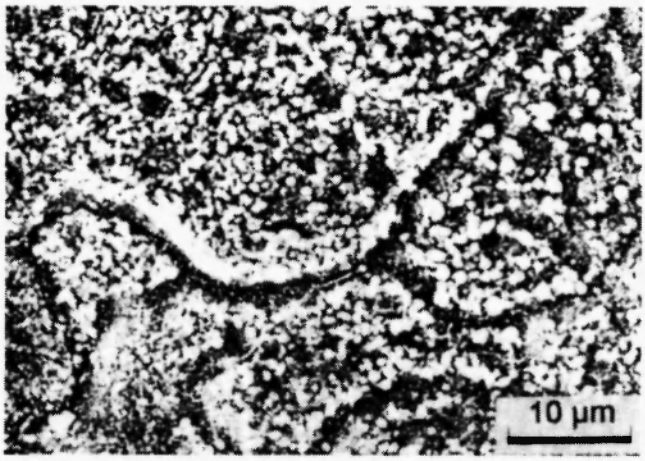

Fig. 5: SEM morphology of the open grain boundaries in the oxidised layer at 600° C.

up to 800° C, the oxide scale is noticeably thicker and more cracked than at lower temperatures (Figure 6). Detachment of the scale may have occurred due to the creation of new surfaces which are energetically more favourable at this temperature than creep of the oxide to maintain adhesion /12/. In this figure, some details of the outer and inner scales are also presented. It can be observed that the inner scale had grown with a porous sponge-shaped morphology, whilst the outer oxide scale showed different crystalline morphologies, with the grain boundaries quite opened. Thus, this structure could confer a non-protective behaviour on the oxide grown under the experimental conditions.

The cross-section morphology of the samples oxidised at 400° C is presented in Figure 7, where the etched alloy, the alloy/oxide scale interface and the layered oxide scale from the left to the right hand side can be seen. No remarkable microstructural changes in the metal phase in comparison to the as-received steel as a result of the heat treatment can be observed. Since chromium was not detected by EDS microanalysis in the oxide phase, an attempt was made to locate this element by electron probe microanalysis. Figure 8 shows the O, Mn, Cr, Fe, Mo, Cu and Si profiles across the oxide/metal phase boundary. It can be seen that Cr, Cu and Mo were incorporated at the interfacial oxide/metal phase boundary, probably as mixed oxides. Si is also incorporated at this interface and in the inner oxide layer.

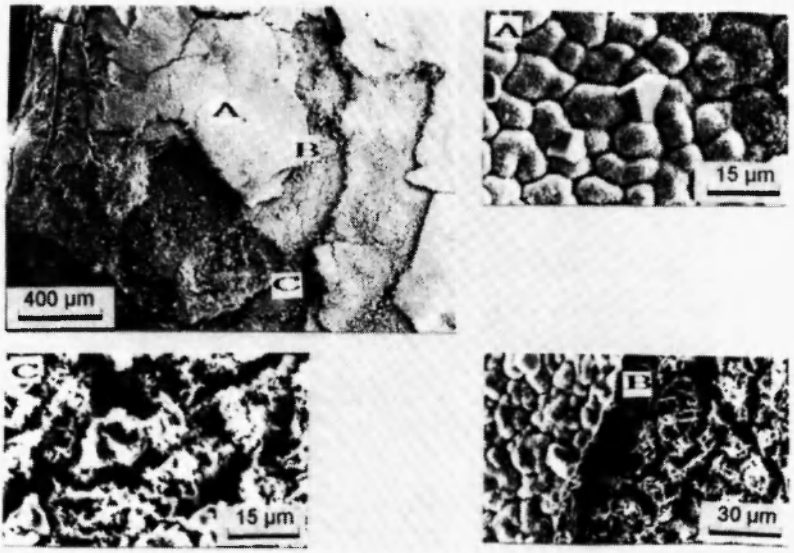

Fig. 6: SEM morphology of the sample treated at 800° C showing some details of the surface oxides.

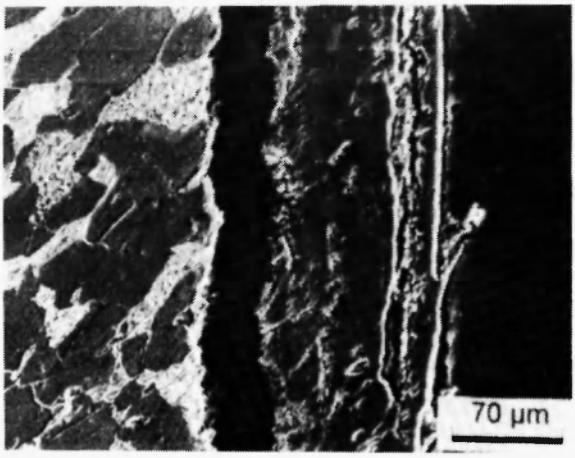

Fig. 7: SEM morphology of the oxide/steel matrix interface at 400° C.

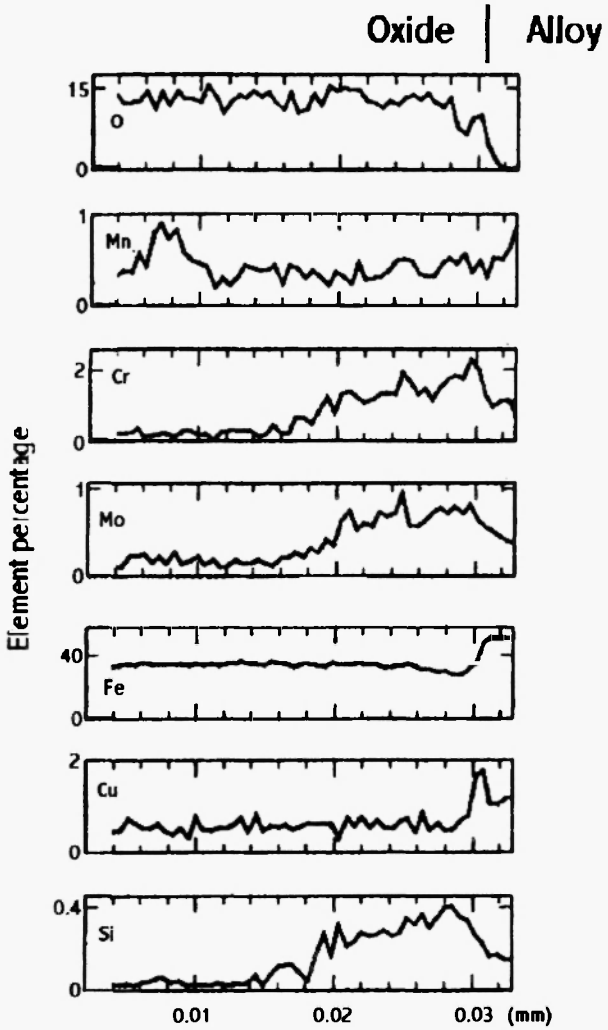

Fig. 8: EPMA of the oxide/alloy interface at 400° C.

The effect of this element was previously reported by Pérez *et al.* /13/ on the same 13CrMo 4 4 steel after its oxidation in air at 700° C up to 144 hours. Otero *et al.* /14/ and Pérez *et al* /15/ presented similar findings for an austenitic AISI 304 stainless steel oxidised at 900° C for the same exposure times and in an air atmosphere.

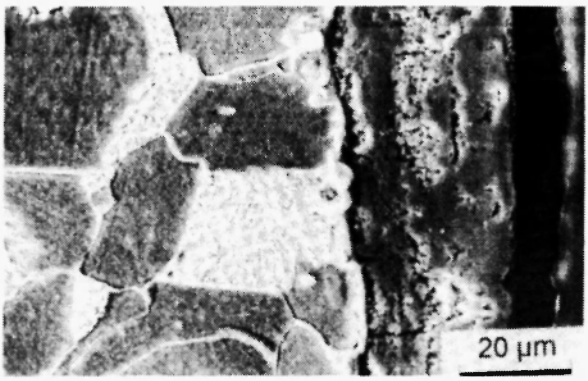

Fig. 9: SEM morphology of the oxide/steel matrix interface at 600° C.

Figure 9 shows the oxide/metal phase boundary at 600° C. The main difference in relation to the sample treated at 400° C is the presence of some isolated iron carbides in the ferritic phase of the steel. Figure 10 depicts the O, Mn, Cr, Fe, Mo, Cu and Si profiles across the oxide/steel boundary obtained by microprobe analysis. Similarly to the 400° C specimen, Cr, Cu, Mo and Si were incorporated into the oxide/metal interface.

On the contrary, a completely different microstructure is observed in the steel oxidised at 800° C (Figure 11). The perlite present in the as-received steel has disappeared and a large number of chromium-iron mixed carbides have appeared in the ferritic steel matrix. On the other hand, the thicknesses of the scale layers hardly increased; three different layers, namely Z1, Z2 and Z3, were observed. These layers have different appearances probably related to their different protective characteristics. Thus, the outer layer (Z3) is the most compact, whereas the inner one (Z1) has a very porous nature. Chromium was detected by X-ray microanalysis in the inner part (Z1) of the scale. Figure 12 shows the O, Mn, Cr, Fe, Mo, Cu and Si profiles on the oxide/steel boundary at 800° C, as obtained by EPMA. At this temperature, Cr and Cu are incorporated at the oxide/metal phase interface, achieving higher concentrations than at lower temperatures as a consequence of their diffusion from the alloy. The Cr concentration is maintained constant (about 5%) across all the oxide layers, giving rise to the presence of $Fe_{1.2}Cr_{0.8}O_3$, which was already detected by X-ray diffraction (Figure 3). Furthermore, Mo is also incorporated in the inner scale layers in an almost constant

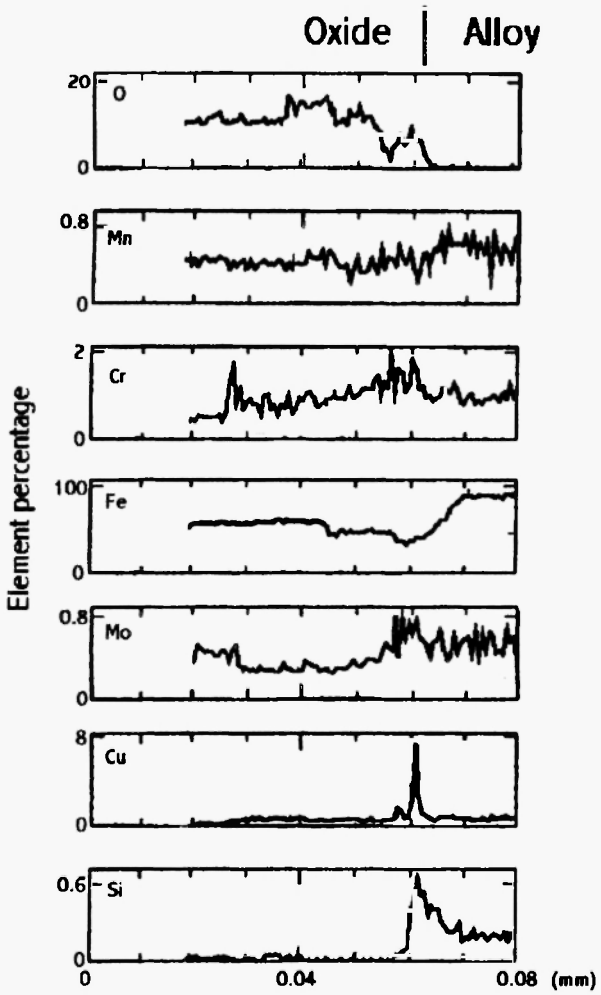

Fig. 10: EPMA of the oxide/alloy interface at 600° C.

concentration (about 1%) across them. Grabke and Meier /16/ reported that molybdenum oxides, such as MoO_2 and MoO_3, would volatilise at temperatures above 600° C. Due to the low Mo content in the scales, this fact would be unlikely to occur, but due to the non-inherent protective properties of the molybdenum oxides, they may perhaps play some detrimental role in the protective characteristics of the oxide layer.

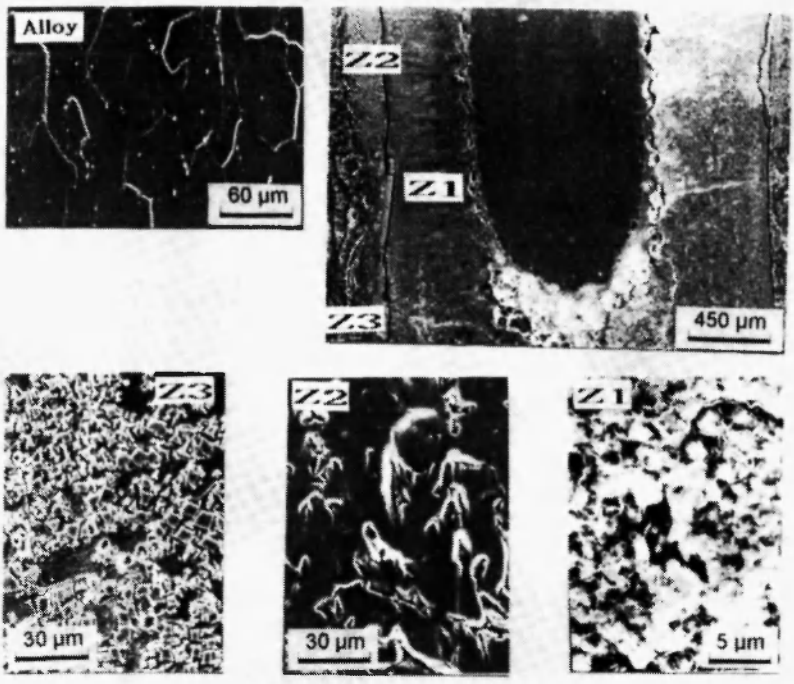

Fig. 11: SEM cross section morphology of the sample oxidised at 800° C. Details of the Z1, Z2 and Z3 oxidised sub-layers.

On the other hand, at all tested temperatures, even considering its small concentration, Mn is diffused towards the oxide layer, probably in the form of a spinel-oxide type, such as that reported by other authors in similar ferritic steels /17/.

CONCLUSIONS

The high temperature corrosion resistance of the 13CrMo44 steel is very satisfactory for temperatures lower than 400° C. Above this temperature a significant increase in the corrosion rate takes place, changing the corrosion mechanism from a parabolic to a paralinear mechanism. According to literature, this steel is able to withstand temperatures of 535° C. Therefore, an

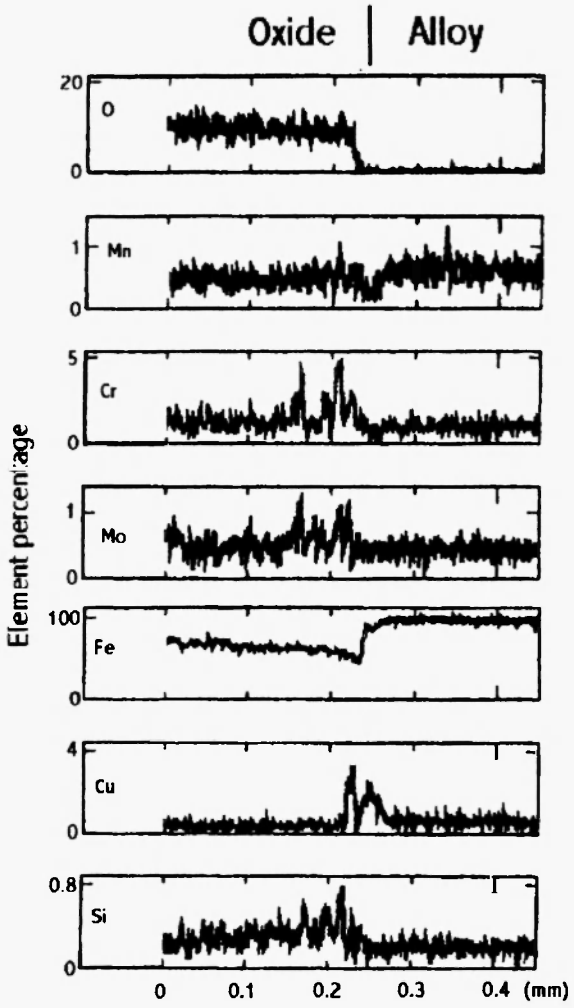

Fig. 12: EPMA of the oxide/alloy interface at 800° C.

oxidation test at lower temperatures than about 550° C would be of interest for purposes of comparison.

For all the tested temperatures, a number of Cr atoms in the outermost part of the alloy may have precipitated as mixed Cr-Fe carbides, resulting in the transformation of perlite to ferrite and chromium-iron carbides. The remaining Cr is mainly incorporated in the inner oxide scale and, thus, this is

thought to provide the highest protection. According to X-ray results, the rest of the scale is mainly composed of Fe_2O_3 and/or Fe_3O_4 with a poorer protective nature than Cr_2O_3. However, for the highest temperatures, it is thought that formation of wustite may have taken place and, upon cooling to room temperature, it has transformed into Fe_3O_4 and α-Fe. The presence of FeO in the oxide scale may have brought about the poorest performance of the alloy under the tested oxidative conditions.

REFERENCES

1. A. Steel, *Handbook for Materials Research and Engineering*, Vol. 2, p. 433, Springer Verlag Stahleisen, (Verein
2. Deutscher Eisenhüttenleute, Ed., Düsseldorf 1992.
3. *Metals Handbook ,Properties and Selection: Irons and Steels.* Vol. 1, p. 639 (9nd Edn) American Society for Metals, Metals Park, Ohio, 1978.
4. C.W. Wegst, *Stahlschlüssel*, p. 63,Verlag Stahlschlüssel Wegst, Marbach, 1992.
5. J. Stringer, *Mat. Sci. Eng*, **87**, 1 (1987).
6. C.J. Franklin and C. Henry, in: *Proc. Materials for Advanced Power Engineering*, Part I, p.89, Kluwer Academic Publishers, Dordrecht, 1994.
7. A. Kumar, in: *10th International Congress on Metallic Corrosion*, Madras, India. Key Engineering Materials, 20-28, 3641, 1988.
8. E. Metcalfe and B. Scarlin, in: *Materials for Advanced Power Engineering*. Part I. p. 35, Jülich, Germany, 1998.
9. B.K. Jha, B.D. Tripathi and V.S.J. Dwivedi, *J. Mat. Sci. Letters*, **15**, 89 (1996).
10. M. Hansen, *Constitution of Binary Alloys*, p. 686, Mc Graw Hill Book Company, Inc; New York, 1958.
11. M. Schütze, in: *Protective Oxide Scales and Their Breakdown*, D.R. Holmes (Ed), John Wiley & Sons, Chichester, 1997; p. 18.
12. F.H. Sttot, G.C. Wood and J. Stringer, *Oxidations of Metals*, **8**, 113 (1995).
13. F.J. Pérez, E. Otero, P. Hierro, C. Gómez, F. Pedraza, J.L. de Segovia and E. Roman, *Surf. & Coatings Technol.*, **108-109**, 121-126 (1998).
14. E. Otero, F.J. Pérez, P. Hierro, C. Gómez, F. Pedraza, J.L. de Segovia, and E. Román, *Revista de Metalurgia*, **34**, 118 (1998).

15. F.J. Pérez, E. Otero, P. Hierro, C. Gomez, F. Pedraza., J.L. de Segovia and E. Román, *Surf.& Coatings Technol.*, **108-109**, 127 (1998).
16. G. H. Grabke and G.H. Meier, *Oxid. Met.*, **8**, 147 (1995).
17. C. Berthier, J.M. Lameille, M. Lenglet, D. Abida, J. Lopitaux and E. Beucher, *Mat. Sci. Forum*, **89**, 251(1997)